The concentration-depth profile at the surface of a solution of tetrabutylammonium iodide in formamide, based on angle-resolved photoelectron spectroscopy

1995 J. Phys.: Condens. Matter 7 1961

(http://iopscience.iop.org/0953-8984/7/10/006)

J. Phys.: Condens. Matter 7 (1995) 1961–1978. Printed in the UK

The concentration–depth profile at the surface of a solution of tetrabutylammonium iodide in formamide, based on angle-resolved photoelectron spectroscopy

F Eschen, M Heyerhoff, H Morgner and J Vogt

Institute of Experimental Physics, Science Department, University of Witten/Herdecke, D-58448 Witten, Germany

Received 14 August 1994, in final form 9 November 1994

Abstract. We have investigated a solution of tetrabutylammonium iodide (TBAI) in the polar solvent formamide (FA) using angle-resolved photoelectron spectroscopy at the Berlin Electron Storage Ring for Synchrotron Radiation (BESSY). The concentration was set to 0.5 molality. We have evaluated the signals from C 1s pertaining to TBAI and FA separately, varying the photon energy between 310 and 540 eV as well as the e-emission angle with respect to the surface normal. The combination of these data with earlier results from ARXPS obtained by Siegbahn and co-workers allowed us to establish a concentration–depth profile of the surface-active salt TBAI. For this purpose we have employed a new theoretical formulation and developed a new elaborate fitting program based on a genetic algorithm. The concentration of the salt could be followed down to a depth of about 45 Å below the surface. Cross sections for the inelastic energy loss of electrons in the liquid could be established as a function of electron energy. Comparison with conventional surface tension measurements allowed us to derive absolute values for the cross sections.

1. Introduction

The surface activity of tetrabutylammonium iodide (TBAI) when dissolved in polar solvents such as formamide (FA) has motivated several electron spectroscopy investigations of this system. Predominantly, these investigations were carried out with photoelectron spectroscopy. Ballard *et al* [1] showed for the first time by ultraviolet photoelectron spectroscopy (UPS) that dissolving TBAI in FA leads indeed to a drastic change in the photoelectron spectrum. More quantitative results were obtained by Siegbahn and co-workers [2, 3]. Using angle-resolved x-ray photoelectron spectroscopy (ARXPS) they could demonstrate that there is no differential segregation between the cations TBA^+ and the anions I^- within the depth resolution of a few Ångströms. A few years later this finding was endorsed by a study using metastable induced electron spectroscopy (MIES) [4]. It was found that MIES is able to detect the anions I^-. As this technique is distinguished by a perfect surface sensitivity, this means that the anions I^- not only are close to the surface but also appear in the topmost layer. Within the experimental uncertainty it was concluded that negative and positive ions are present at the surface itself in equal amounts. This is by no means an obvious statement; if the iodide ion I^- is exchanged for a similar ion Br^-, the situation changes drastically; again using MIES, it was shown that the concentration of the anion in the topmost layer is even below the bulk concentration, whereas the cation TBA^+ is only slightly less abundant at the surface itself compared with the iodide salt [5].

0953-8984/95/101961+18$19.50

In conclusion we may state that the segregation of the salt TBAI to the surface of a FA solution occurs in the same way for both ions. From indirect evidence, one can even assume [4, 5] that ion pairs rather than individual ions diffuse to the surface.

As the enhancement of the salt concentration at the surface itself is established, the next goal should be the evaluation of its concentration–depth profile. The first to do this were Holmberg *et al* [3]. They tried two analytical shapes for the depth profile: a step function and an exponential function to describe the excess number density of the salt near the surface. In both cases, two parameters are to be determined. From these results, one can estimate the thickness of the layer of enhanced concentration between 6 and 11 Å. Given the diameter of the positive ion TBA^+ which is about 9.5 Å, this finding suggests that the enhanced salt concentration is confined to a depth which corresponds to the thickness of one monolayer of salt. Increasing or decreasing the TBAI bulk concentration appears to affect merely the salt fraction of the surface layer. From MIES data [4] we conclude that at a bulk concentration of unit molality a little over half the surface area is covered by salt. This corresponds to an enhancement of the salt-to-solvent ratio at the surface by a factor of 6 over the bulk value. At lower bulk concentrations the enhancement factor reaches values up to 15. In [4] the surface salt concentration was claimed to depend on temperature between 0.2 and 0.5 molal bulk concentration. A later investigation could not reproduce the effect, but ended with a rather smooth and temperature-independent relation between the surface and bulk concentration [6]. The quantitative evaluation of the salt concentration profile was repeated recently for a 0.5 M TBAI–FA solution, based on an augmented set of experimental data. The ARXPS data of Siegbahn and co-workers were combined with our own results from angle-resolved valence electron spectroscopy (ARUPS) and with MIES from [5]. The notion that the segregation does not extend into the liquid beyond the thickness of a salt monolayer was again endorsed.

In the present paper we evaluate for a 0.5 M solution (i.e. 0.5 mol salt (kg solvent)$^{-1}$) of TBAI in FA the concentration–depth profile with improved accuracy. Progress has been achieved in two respects. Firstly, we have once again increased the number of input data substantially using C 1s core electron spectroscopy; by varying the photon energy and the angle between the surface normal and the direction of electron detection we were able to vary the effective observation depth by 1.5 orders of magnitude. Thus, our data are sensitive to all separations from the surface which are relevant for establishing a concentration profile.

Secondly, we have developed a new computer program for fitting the depth profile to the experimental data. The program is based on a genetic algorithm [8]. For the present purpose we found this fitting strategy to be impressively powerful. It searches a parameter space much larger than could be allowed for in a previous study [7]. This means that a very flexible model with a large number of parameters can be employed. The danger of ending up with an arbitrary solution was nonetheless successfully avoided. On the contrary, we have established an internal criterion for the uniqueness of our result and we believe that we are the first to do so in the field of depth-profiling electron spectroscopy.

The paper is organized as follows: the next two sections describe the experimental set-up and the theory employed in the data evaluation. Section 4 presents our experimental results and the depth profile derived thereof. Further we discuss the physical picture of the surface and relate it to information from other methods.

2. Experimental details

The measurements were carried out with a machine especially designed for the purpose of studying liquid surfaces with synchrotron radiation (figure 1). During operation of the liquid

target the pressure in the main chamber easily reaches 10^{-2} Pa. Therefore two differential pumping stages are required between our experiment and the storage ring, the first stage being equipped with a cold trap in addition to a turbomolecular pump. Further, a glass tube of 6 mm diameter and 150 mm length represents an efficient resistance to the vapour flow while not interfering with the beam of synchrotron radiation. These measures keep the pressure in the two differential pumping stages below 10^{-6} Pa and 10^{-7} Pa under all working conditions.

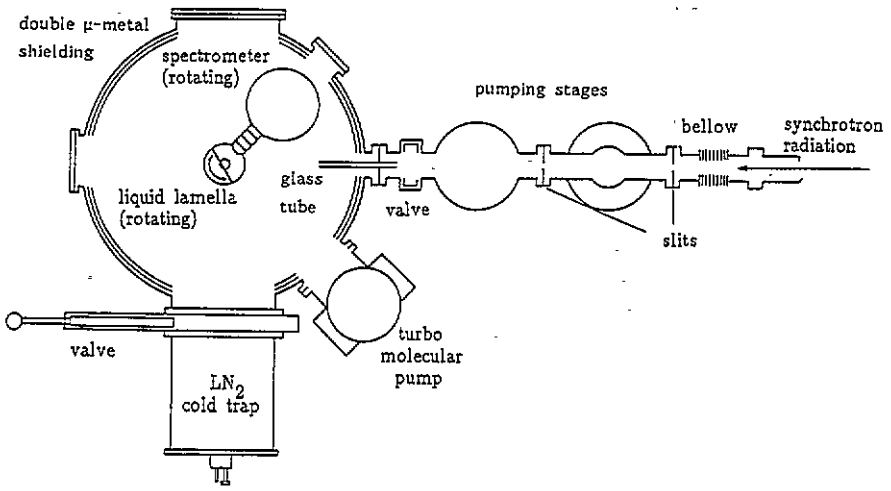

Figure 1. Cross section of the machine. The main chamber is separated from the storage ring by two differential pumping stages. The synchrotron radiation enters the main chamber through a 150 mm glass tube of 6 mm diameter. The liquid lamella can be rotated about the central axis of the chamber in order to vary the angle between the photon beam and the normal of the liquid surface. The differentially pumped electron spectrometer rotates about the same axis.

The main chamber has the shape of a standing cylinder with a diameter of 50 cm. A turbomolecular pump (Balzers; 330 l s^{-1}) achieves a background pressure of about 10^{-4} Pa. During operation of the liquid target a LN_2 cold trap acts as cryopump for the vapour with a pumping speed of about 3000 l s^{-1}. Double μ-metal shielding reduces the magnetic field in the centre of the chamber to less than 3 mG. This is sufficient to perform angle-resolved UPS measurements even at very low electron energies. The electron spectrometer is of the pseudo-spherical type (Comstock AC 902 with a channel-plate detector). It is housed in a differentially pumped chamber which rotates about the vertical centre axis of the main chamber.

The liquid target is shown in figure 2. The liquid flows out of eight demagnetized hypodermic needles into the groove of a stainless steel plate. The shape of the groove has been designed by trial and error so as to ensure that an area of about 5 mm diameter has a stable flat liquid surface which is a prerequisite for angle-resolved studies. The liquid target can be rotated about the same axis as the electron spectrometer. Thus, the angles between the surface normal and the light beam on one side and between the surface normal and the electron spectrometer on the other side can be set independently. The only shortcoming is the fact that the still somewhat bulky shape of the spectrometer chamber requires a minimum

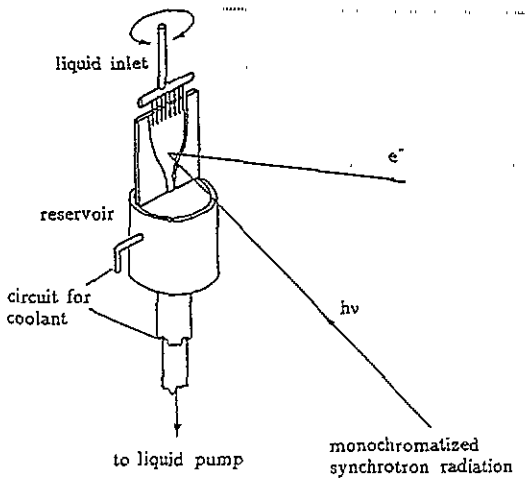

Figure 2. A 3D view of the liquid lamella. The liquid enters from above and is guided by eight demagnetized hypodermic needles into the groove of a stainless steel plate. The area illuminated by the synchrotron radiation appears as a flat and stable surface. The liquid is collected in a reservoir and flows under gravity down to a centrifugal pump. From there it is pushed via a stainless steel tube again to the liquid lamella. The liquid circuit has a double wall where possible to allow cooling.

angle between the light beam and the direction of e^- detection of 40°. We hope to improve this in the future.

The chemicals TBAI and FA were purchased from Jansen Chimica and used without further purification. The mean impurity in FA could be water. However, in previous experiments we found no trace of water at the FA surface even when several per cent of H_2O were added [9].

3. Theory

3.1. The concentration–depth profile

Our previous attempts to evaluate concentration depth–profiles [7, 10] were based on three assumptions.

(1) The solution is compact up to the surface, i.e. the molecules of all species always fill the same volume.

(2) The electron mean free path λ does not depend on the relative abundance of the species, i.e. it is a constant value from the bulk up to the surface itself.

(3) The observation depth λ' varies linearly with the cosine of the e^- emission angle θ, i.e. $\lambda' = \lambda \cos\theta$.

In the meantime we have learned about the depth-profiling framework developed by Baschenko [11]. Since Baschenko does not need to rely on the first two assumptions, we find his formulation clearly superior and adopt it in the following. Thus, the first two assumptions are not needed in the following. The treatment of assumption (3) in [11] will be discussed below. Two further assumptions which are made here and in other work [7, 10, 11] are as follows.

(4) Beyond a finite separation from the surface the liquid retains its bulk composition and structure.

(5) The range between this separation and the surface itself is conceived as being sliced into a number of parallel layers. The important assumption made is that every one of these layers has a homogeneous composition, vertically and laterally. Since we deal with molecules whose size is the same order of magnitude as the thickness of the layers, this assumption is necessarily unphysical. We do not have the impression that the consequences of this assumption are overly severe. However, it appears worthwhile to devote some effort to this problem in the future; its solution may offer insight not only into the composition but also into the structure of the top layers.

We list some necessary definitions: i, k, indices of species that are distinguished in the liquid, $i, k \in [1, i_{\max}]$; j, index of layers, $j = 1$ indicating the topmost layer, $j \in [1, j_{\max}]$; d_j, thickness of layer j; q_i photoionization cross section of species i, which depends on the orbital ionized, on the photon energy and light polarization (since we evaluate only signal ratios from C 1s orbitals, these dependences are not relevant in the present study); $\sigma_i(E)$, cross section for inelastic energy loss of photoelectrons due to a molecule of species i, which depends on the electron energy E; $n_i(j)$, number density of species i in layer j; $N_i(j) = n_i(j)\sigma_i / \sum_k n_k(j)\sigma_k$ with $\sum_k N_k(j) = 1$, parameter introduced by Baschenko [11], useful for carrying out the actual fitting procedure; $c_i(j) = n_i / \sum_k n_k(j)$ with $\sum_k c_k(j) = 1 = [N_i(j)/\sigma_i] / \sum_k [N_k(j)/\sigma_k]$; $\lambda_j(E) = 1 / \sum_k n_k(j)\sigma_k(E)$, mean free path of electrons in layer j which depends on the electron energy E by virtue of the energy dependence of the cross sections $\sigma_k(E)$; $\lambda'_j(E, \theta) = f(E, \theta)\lambda_j(E)$, observation depth as a function of emission angle; $t_j(E) = d_j/\lambda_j(E)$, reduced thickness of layer j, which depends on the electron energy by virtue of $\lambda_j(E)$.

All quantities referring to bulk properties are labelled by a superscript b, e.g. n_i^b is the number density of species i in the bulk, c_i^b is the molar fraction of species i in the bulk and $N_i^b = n_i^b\sigma_i / \sum_k n_k^b\sigma_k$ is Baschenko's parameter of species i in the bulk.

Using the above definitions we can write the contribution of species i in layer j to the signal as

$$I(i, j, \theta) = q_i n_i(j)\lambda'_j(E, \theta)\left[1 - \exp\left(-\frac{d_j}{\lambda'_j(E, \theta)}\right)\right]\prod_{j'=1}^{j-1}\exp\left(-\frac{d_{j'}}{\lambda'_{j'}(E, \theta)}\right). \tag{1}$$

The respective contribution from the bulk below the range of the explicitly treated layers is

$$I(i, \text{bulk}, \theta) = q_i n_i^b \lambda'^b(E, \theta)\prod_{j=1}^{j_{\max}}\exp\left(-\frac{d_j}{\lambda'_j(E, \theta)}\right). \tag{2}$$

Employing Baschenko's parameters $N_i(j)$, we can rewrite both expressions to give

$$I(i, j, \theta) = \frac{q_i}{\sigma_i} f(E, \theta) N_i(j)\left[1 - \exp\left(-\frac{t_j}{f(E, \theta)}\right)\right]\exp\left(-\sum_{j'=1}^{j-1}\frac{t_{j'}}{f(E, \theta)}\right) \tag{3}$$

and

$$I(i, \text{bulk}, \theta) = \frac{q_i}{\sigma_i} f(E, \theta) N_i^b \exp\left(-\sum_{j=1}^{j_{\max}}\frac{t_j}{f(E, \theta)}\right). \tag{4}$$

The total signal from species i at emission angle θ is then

$$I(i,\theta) = \sum_{j=1}^{j_{max}} I(i,j,\theta) + I(i,\text{bulk},\theta). \tag{5}$$

The experimental data consist of signal ratios from different species, say i and k. The corresponding theoretical quantities are obtained as

$$R_{i,k}(\theta) = I(i,\theta)/I(k,\theta). \tag{6}$$

The above formulation deviates from Baschenko's concept [11] in two respects. There the θ-dependence has throughout the special form

$$f(E,\theta) = \cos\theta \tag{7}$$

but this does not mean that the simple concept of the mean free path is maintained. In contrary, in [11] the correction factors $B_i(j)$ are introduced into equations (1) and (3). They account for the fact that elastic scattering may obscure the simple dependence of the signal on the angle θ, given by equation (7). The correction factors $B_i(j)$ have to be supplied before a fit to experimental data can be started. The calculation of these factors is performed by Monte Carlo trajectory calculations [11]. For electrons of about 1200 eV energy the B-factors are found to deviate from unity by up to 30%. Much larger deviations are observed as well, but only for situations that almost do not contribute to the signal, e.g. for deep layers and large emission angles θ. The introduction of the factors B means that effectively the concept of a mean free path is abandoned. This follows from the fact that the contributions from different layers cannot be conceived any longer as being weighted by an exponential function of the separation from the surface. It is interesting to note that the experience gained when reconstructing the depth profile of a polyurethane film on a gold substrate [11] indicates that the main advantage of Baschenko's new *ansatz* does not rest in the employment of the correction factors $B_i(j)$ but rather in the concept of a mean free path whose value depends on the local composition. Similar conclusions had to be drawn from the depth profiling at a liquid surface based on C 1s ARXPS data [12]. Therefore, we have omitted in the above treatment the correction factors B. We had to deal, however, with another phenomenon. Our experimental data were taken with many different photon energies. The resulting electron energies vary between 17 and 247 eV. In addition we have incorporated in the data set the XPS results obtained by Siegbahn and co-workers [3] with an electron energy of 1200 eV. It is obvious that the electron mean free path must strongly vary over this large range of electron energies. No reliable scaling law exists that could link the path lengths. We solved the problem by introducing the ratios

$$\lambda(E)/\lambda(E_{XPS}) \tag{8}$$

as additional parameters into the fitting procedure, E_{XPS} being the kinetic energy from the XPS data. Finally, we have considered the possibility that equation (7), while proving appropriate for the energy $E_{XPS} = 1200$ eV [12, 13], may not be a suitable choice for much lower electron energies. Indeed, a good fit to all data could be obtained only after replacing the linear relation (7) by the polynomial *ansatz*

$$f(E,\theta) = a(E) + b(E)\cos\theta + c(E)\cos^2\theta \tag{9}$$

with

$$a(E) + b(E) + c(E) = 1.$$

At the beginning we made the coefficients a, b and c explicit functions of the electron energy E. We found, however, that the coefficients did not show a systematic energy dependence for low energies 17 eV $\leqslant E \leqslant$ 247 eV. Thus, we finally chose

$$f(E,\theta) = \begin{cases} a + b\cos\theta + c\cos^2\theta \\ \cos\theta \end{cases} \quad \text{for} \quad \begin{cases} E \leqslant 247 \text{ eV} \\ E = 1200 \text{ eV} \end{cases} \tag{10}$$

It is interesting to note that in all runs the coefficients a and b were assigned small values, which means that the behaviour of $f(E,\theta)$ is dominated by the quadratic term. This indicates that the observation depth

$$\lambda'(E,\theta) = f(E,\theta)\lambda(E)$$

falls off more rapidly with increasing emission angle than anticipated from the simple relation

$$\lambda'(\theta) = \cos\theta\lambda$$

which appears to hold reasonably well only at high electron energies. Beyond our main goal, namely to establish a concentration–depth profile, this piece of information is very interesting in itself, since there is no theoretical treatment available about the behaviour of slow but still free electrons in a liquid or near its surface.

Similar to previous work [7] we shall establish a relation between the concentration profile and the surface excess which can be determined from surface tension measurements via the Gibbs equation [15]. For this purpose we have to evaluate the total amount of species i in any of the layers j:

$$\Gamma_i(j) = n_i(j)d_j.$$

Neither of the factors on the right-hand side is obtained in the fitting procedure. Therefore we rewrite the above expression as

$$\begin{aligned} \Gamma_i(j) &= n_i(j)\lambda_j d_j/\lambda_j \\ &= [N_i(j)/\sigma_i]t_j. \end{aligned} \tag{11}$$

In practice we do not know the cross sections σ_i for inelastic energy loss but rather the ratio of the two species. Let us assume that all cross sections are known in units of the cross section pertaining to species 1, say the solvent. We find that

$$\Gamma_i(j) = \frac{1}{\sigma_1}\frac{N_i(j)}{\sigma_i/\sigma_1}t_j. \tag{12}$$

The parameters $N_i(j)$ are obtained in the fit, the reduced layer depth t_j is set before the fit starts (in our case, all layers are given the same reduced thickness $0.05 = t = t_j$, $j = 1, \ldots, j_{\max}$) and the ratios σ_i/σ_1 are either known from other sources or determined

in the fit as well. The only unknown on the right-hand side is then σ_1. Except for the prefactor $1/\sigma_1$ the absolute amount for the species i per unit area in layer j is then determined. Summing over all layers, we get

$$\Gamma_i = \frac{1}{\sigma_1} \sum_{j=1}^{j_{max}} \frac{N_i(j)}{\sigma_i/\sigma_1} t_j. \tag{13}$$

The measurement of the surface tension γ as a function of bulk composition can be related to the above quantities via the Gibbs equation [15]. For a binary system this is

$$-\frac{d\gamma}{d\mu_2} = \Gamma_2 - \frac{c_2^b}{c_1^b}\Gamma_1 \tag{14}$$

where μ_2 is the chemical potential of species 2, say the dissolved salt, and the c_i^b denote the bulk molar fractions. The chemical potential μ is related to the activity a by

$$\mu = RT \ln\left(\frac{a}{a_0}\right)$$

where $R = 8.314$ J mol^{-1} K^{-1} is the Boltzmann constant multiplied by Avogradro's number N_A and T is the temperature in Kelvin. At low concentrations the activity a is proportional to the molar fraction c according to Raoult's law [15] which leads to

$$-\frac{c_2^b}{RT}\frac{d\gamma}{dc_2^b} = \Gamma_2 - \frac{c_2^b}{c_1^b}\Gamma_1. \tag{15}$$

When we define the Gibbs dividing plane as lying between the deepest layer of our model and the bulk we can identify the Γ_i from equation (15) with the quantities in equation (13) and obtain

$$-\frac{c_2^b}{RT}\frac{d\gamma}{dc_2^b} = \frac{1}{\sigma_1}\sum_{j=1}^{j_{max}}\left(\frac{N_2(j)}{\sigma_2/\sigma_1} - \frac{c_2^b}{c_1^b}N_1(j)\right)t_j. \tag{16}$$

The left-hand side of this equation can be determined from conventional surface tension measurements whereas all quantities except σ_1 on the right-hand side can be assessed by electron spectroscopy via the depth-profiling procedure. Accordingly, we have the unique possibility of determining the absolute cross section of the solvent molecule for electron energy loss in the liquid phase. The corresponding cross section for the other species is then readily obtained from the ratio σ_2/σ_1. Note that except for σ_1 all quantities on the right-hand side of equation (16) are dimensionless. Accordingly, the units of σ_1 are determined by the convention chosen on the left-hand side of the equation.

The energy dependence of σ_1 is given by the energy dependence of $t_j(E)$. It follows that $\sigma_1(E)$ can be derived from the ratios

$$\lambda_j(E)/\lambda_j(E_{XPS})$$

which are explicitly used as parameters in the fitting procedure. Note that these ratios do not depend on E in the present framework even though the mean free path $\lambda_j(E)$ itself does. We get

$$\sigma_1(E) = \sigma_1(E_{XPS})\frac{\lambda_j(E_{XPS})}{\lambda_j(E)}. \tag{17}$$

The energy dependence of the other cross sections is then obtained as

$$\sigma_i(E) = \sigma_1(E)\frac{\sigma_i}{\sigma_1} \tag{18}$$

where the ratio σ_i/σ_1 is considered to be independent of the electron energy.

3.2. Requirements for the fitting procedure

We can summarize now the task that we have to perform in the fitting procedure.

We consider explicitly 30 layers. Since no hint for differential segregation between the positive and negative ions has been observed, as discussed in the introduction, we can describe the composition of every layer by only one parameter $N_{\mathrm{TBAI}}(j)$. The corresponding parameter $N_{\mathrm{FA}}(j)$ for the solvent follows from the normalization relation of these parameters (see definitions above).

As our data set contains results with ten different electron energies $E < E_{\mathrm{XPS}}$ we have to fit ten additional parameters $\lambda(E)/\lambda(E_{\mathrm{XPS}})$, (cf equation (8)). The polynomial for the angle dependence (equation (10)) requires two more parameters; we have chosen b and $a/(a+c)$. Finally we have fitted the ratio of the cross sections for inelastic scattering:

$$\sigma_{\mathrm{TBAI}}/\sigma_{\mathrm{FA}}. \tag{19}$$

Even though both cross sections depend on the electron energy we assume that their ratio does not. From gas-phase electron impact cross sections there exists impressive evidence that this is a very good approximation [14]. In total we count no less than 43 unknowns that we are going to determine in the fitting procedure. Two questions arise at this point.

(1) Which algorithm is able to find a good solution in this large parameter space without a 'good guess' as a starting condition?

(2) Is there any internal measure for the uniqueness of the solution found?

The answer to question (2) is linked to question (1). Let us assume that we had an algorithm which is able to search the full parameter space associated with the problem and is able to find a good solution in a finite interval of time irrespective of the starting conditions. The next step is to carry out the search for as many different starting values as possible. The spectrum of parameter sets obtained in this way then decides the extent to which one can speak of a solution and its error margins or whether no identifiable solution exists at all.

We have to discuss now whether we can define the full parameter space of our problem. The positive answer can be derived from the fact that all parameters are defined in such a way that they vary only within the interval [0, 1]. The only exception is the ratio of the cross sections, namely $\sigma_{\mathrm{TBAI}}/\sigma_{\mathrm{FA}}$ for which we had to choose (necessarily arbitrary) bounds. Accordingly, we were very observant that the fitted values for this parameter never came near the limits of the chosen interval. We believe that in this way we could ensure that in no run was any possible solution discarded beforehand.

We have repeated the fitting routine a hundred times with starting conditions every time chosen by a random-number generator. As any run of the genetic algorithm produces several different solutions, we had stored at the end several thousands of parameter sets which fulfil the condition to reproduce the experimental data with the experimental uncertainty. From these parameter sets the mean values and the standard deviations of all parrameters were computed. The computing time for the whole procedure is about 36 h on a SPARC station 10-41. The computational effort is certainly very large, but it is justified nonetheless; it is rather obvious that any influence of the investigator and his expectations is almost perfectly excluded during the fitting procedure. In a problem as delicate as depth profiling this is certainly an important point. Genetic algorithms have even been claimed to be an objective mechanism for decisions [16]. One has to realize, however, that in setting up the model (e.g. our introduction of the function $f(E, \theta)$ in equation (10) or the choice of the number of layers) non-objective decisions cannot be totally avoided.

Finally, we discuss the observation that the parameters $N_i(j)$ show large standard deviations if evaluated as independent quantities. One can show, however, that a large degree of correlation between $N_i(j)$ in adjacent layers holds. This can be deduced from the fact that the quantities Γ as defined in equation (13) have very small standard deviations. Thus, the fairly large number of parameters denoted $N_i(j)$, $j = 1, \ldots, j_{\max}$ (in our case $j_{\max} = 30$) could in principle be replaced by a much smaller number of uncorrelated parameters. However, we have not found a systematic way to define such parameters. Instead, we have simply introduced a side condition in the fit. The expression

$$C = \sum_{j=2}^{j_{\max}-1} |N_i(j-1) - 2N_i(j) + N_i(j+1)|g(j) + |N_i(j_{\max}-1) - 2N_i(j_{\max}) + N_i^{\mathrm{b}}|g(j_{\max}) \tag{20}$$

is a measure for the curvature of the fitted profile. The smallness of this expression is employed as an additional criterion for the acceptance of a parameter set as solution. The weighting factor

$$g(j) = j$$

was introduced in order to keep the influence of this criterion near the surface low. This corresponds to the fact that the experimental data are influenced most by the composition close to the surface rather than by the composition of deep layers. Consequently, the parameters of deep layers are determined by the experimental data to a lesser extent than those of the upper layers.

A second criterion was defined as

$$U = \sum_{j=2}^{j_{\max}} |N_i(j) - N_i(j-1)|. \tag{21}$$

This quantity measures the monotonic nature of the profile. It is employed in the course of the fitting calculation at a different stage compared with C. This is discussed below.

The criterion appropriate for a good fit is given as the averaged squared relative deviation between experimental data and their fitted counterpart:

$$D = \frac{1}{M} \sum_{m=1}^{M} \left(\frac{R_{i,k}(E_m, \theta_m)}{R_{i,k}^{\exp}(E_m, \theta_m)} - 1 \right)^2. \tag{22}$$

3.3. The genetic algorithm used

Genetic algorithms have been described in the literature [8, 16, 17] as powerful tools for searching large parameter spaces. Here, we shall briefly outline the features of our program.

Throughout the calculations we have used 1000 individuals per generation, i.e. 1000 parameter sets. Every parameter is coded by 8 bits which allows a relative resolution of 3.92×10^{-3}. Initial tries with higher resolution (10 bits) did not give better results. All individuals are ranked according to the size of the quantity

$$D + C\epsilon. \tag{23}$$

The size of ϵ controls the relative importance of the 'curvature' C (see equation (20)) versus the deviation between fit and experiment (see equation (21)). Several tests suggested $\epsilon = 3 \times 10^{-5}$, the value not being critical. Thus ϵ is used as a strategic parameter to guide the fit and is itself not subject to fitting. The 500 best individuals of a generation are employed to generate the following one by crossing over. The rate of mutation is itself subject to fitting. 5 bits in any individual are reserved to code its probability for mutation. The probability is allowed to vary between 10^{-5} and 10^{-2} on a logarithmic scale. Values of around 10^{-3} were observed in successful individuals. As the total number of bits per individual is 349, this corresponds to about one mutation in every third individual. The actual occurrence of a mutation is decided in the standard way by comparison with a random number.

We have followed the fit over 350 generations, the most successful individuals becoming very similar at this stage.

As mentioned above, we have started the whole procedure up to 100 times with different starting generations in order to explore as fully as possible all parts of the parameter space that yield values for equation (22) below a pre-set value. Both terms of this expression are stored separately with the parameter set. Among the stored parameter sets we select only those that deviate from the experiment by less than the estimated experimental error. Several thousand sets fulfil this condition.

The parameter sets obtained in this way represent the basis for our further treatment. We evaluate the mean and the standard deviation for every fitted parameter. To control the unphysically large variation of the $N_i(j)$, we apply the criterion from equation (21) in order to make a selection from the stored parameter sets. The number of accepted parameter sets drops with decreasing U and finally becomes zero. The decision for the appropriate U is found in the following way: we use the lowest value of U which does not noticeably affect the mean values of the parameters $N_i(j)$. We would like to comment on two points. Firstly, the criterion of equation (21) is not active during the search of the genetic algorithm and thus does not exclude any solution from contributing to the mean values of the parameters $N_i(j)$. Secondly, avoiding unphysical jumps of the concentration between the layers by the above method is certainly superior to simple smoothing. This not only could wash out structure but also could produce profiles that no longer represent the experimental data within the experimental uncertainty.

4. Results and discussion

Photoionization of the C 1s core electrons of the 0.5 M solution of TBAI in FA results in spectra as shown in figure 3. The chemical shift allows us to evaluate separately the relative intensities due to the salt and the solvent. Gas-phase contributions from the solvent can be distinguished as well. The ratio of the peak area of TBAI to that of liquid FA are determined for many combinations of photonenergies and observation angles. The data are given in table 1. Included are the results obtained by Siegbahn and co-workers [3] as we make use of them in fitting the salt concentration profile. The experimental uncertainty is estimated to be better than 8%. Accordingly, we have accepted in the fitting procedure all parameter sets with $D \leqslant 0.006$ (cf equation (22)) as valid solutions. The reduced layer thickness for the largest electron energy $E_{XPS} = 1200$ eV was set to $t_j(E_{XPS}) = 0.05$ for all layers. The number of layers was tried out in several runs. Values of j_{max} between 10 and 40 were employed. It became obvious that the results depend on j_{max} as long as j_{max} is too small. Saturation is reached below $j_{max} = 30$. This number of layers was used for the fit. At the

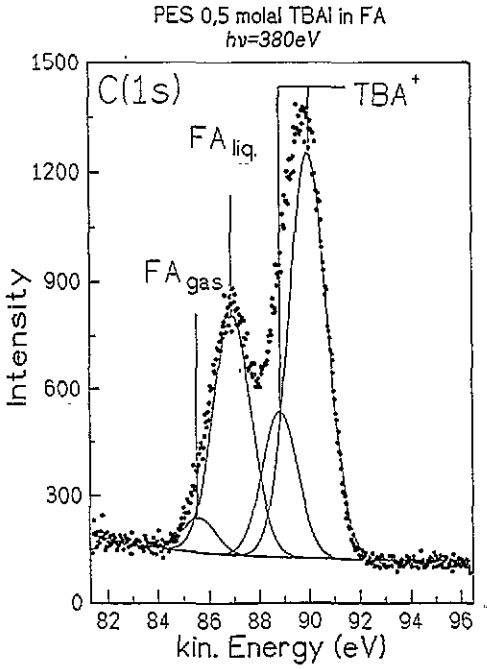

Figure 3. C 1s core electron spectrum of 0.5 TBAI–FA taken at the HE TGM1 monochromator at BESSY. The energy of the photons is $h\nu = 380$ eV with an energy spread of 1 eV. The emission angle of the electrons is $\theta = 15°$. The contributions from TBAI, FA_{liq} and FA_{gas} are indicated. The C 1s signal from Bu_4N is split into two components, the smaller being due to the C atoms close to the nitrogen ion.

end we shall see that the thirtieth layer ends about 45 Å below the surface. Apparently bulk properties are recovered at this depth.

More than 13 000 parameter sets were found which fulfil the criterion $D \leqslant 0.006$. As described in the previous section, we reduced the number of parameter sets with the aid of quantity U from equation (21). Requiring an upper limit of U leads to a reduced scatter of the parameters $N_i(j)$. The lowest value of U is chosen which does not yet affect the mean values. This is demonstrated for two quantities in figure 4. The reduced surface excess and the ratio $\sigma_{TBAI}/\sigma_{FA}$ remain fairly stable down to $U = 0.5$. The same observation holds for $N_i(j)$, but in their case the standard deviation decreases noticeably with increasing U which is the desired effect. The number of surviving parameter sets as a function of U can be found from figure 4 as well. $U = 0.5$ was employed for the results presented in the following. Table 2 shows several quantities that can be assessed in the fit.

The concentration profile expressed by the TBAI molar fraction $C_{TBAI}(j)$ is shown in figure 5. The last layer represents the bulk value. The strong enhancement of the salt near the surface is clearly shown in agreement with its known surface activity in polar solvents. The large salt concentration in the top layer falls off sharply to the fourth layer; a few layers (fourth to sixth) follow with a rather constant molar fraction. A drop to 50% of this value is reached after the eighth layer. The thickness of the thus defined range of enhanced salt concentration can be estimated to be about 12 Å, based on $\lambda(E_{XPS})$ from table 2 and $t(E_{XPS}) = 0.05$. From the fifteenth layer to the twenty-seventh layer the salt molar fraction is slightly but significantly smaller than in the bulk. Thus, the salt-rich surface range is followed by an equally broad depletion zone.

Table 1. Ratio of TBAI C 1s signal to FA C 1s signal as a function of energy and emission angle with respect to surface normal. The data with $h\nu = 1486$ eV are taken from [3].

Photon energy (eV)	Electron energy (eV)	Emission angle (deg)	Ratio of TBAI C 1s to FA C 1s
310	17	0	2.85
		30	3.67
		45	3.87
330	37	0	2.54
		30	3.34
		45	3.58
350	57	0	2.21
		30	2.93
		45	3.74
360	67	30	3.03
		45	3.32
370	77	0	1.93
		30	2.3
		45	2.7
380	87	15	2.17
		30	2.5
		45	2.81
390	97	0	1.82
		30	2.35
		45	2.62
440	147	30	2.33
		45	2.29
480	187	0	1.78
		30	1.98
		45	2.35
540	247	0	1.63
		30	1.8
		45	2.1
1486	1193	35	0.82
		60	1
		80	1.8

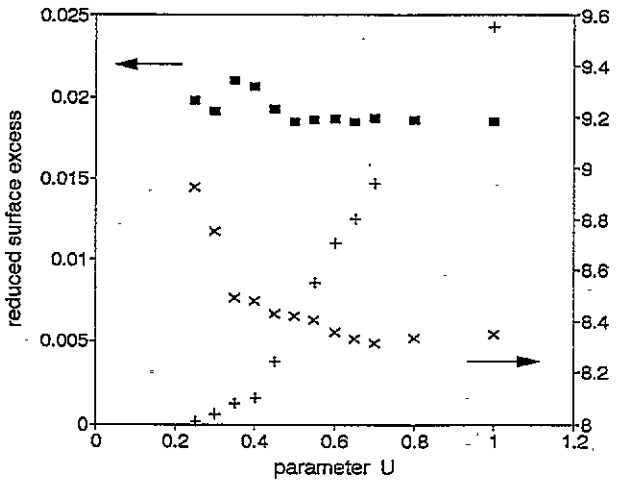

Figure 4. Selected fitted values as function of U which is defined in equation (21). The reduced surface excess $\sigma_{FA}(\Gamma_{TBAI} - (c^b_{TBAI}/c^b_{FA})\Gamma_{FA})$ is defined in equations (13), (15) and (16), the cross section ratio $\sigma_{TBAI}/\sigma_{FA}$ is found in equations (12), (18) and (19). Both quantities remain constant at large values of U but begin to show a distinct U-dependence below $U = 0.5$. The number of accepted parameter sets (+) drops continuously with decreasing U. The final results of this paper are obtained by setting $U = 0.5$. For further discussion see text.

Table 2. Selected values from fit. Errors refer to the standard deviation as explained in the text. The uncertainty originating from the surface tension measurement is estimated to ±15% and is not included in the quoted error of σ_{FA}, λ and λ_M.

Quantity	Value	Unit	Remark
b	0.025(51)	—	See equation (10)
$a/(a+c)$	**0.016(20)**	—	**See equation (10)**
$\sigma_{TBAI}/\sigma_{FA}$	8.42(30)	—	See equations (12), (18) and (19)
$\sigma_{FA}[\Gamma_{TBAI} - (c^b_{TBAI}/c^b_{FA}\Gamma_{FA}]$	0.0185(24)	—	See equations (13), (15) and (16)
σ_{FA}	2.16(27)	10^{-20} m^2	Equation (16), $E_{el} = 1200$ eV
λ^a	30.8(3.9)	10^{-10} m	$E_{el} = 1200$ eV, for bulk FA
λ^b_M	3.45(4.1)	mg m^{-2}	$E_{el} = 1200$ eV, for bulk FA, equation (24)

[a] The number density of bulk FA is 1.5×10^{28} m^{-3}.

[b] $\lambda_M = (m_{FA}/\sigma_{FA})/N_A$ where m_{FA} is the molar weight of FA and N_A Avogadro's number.

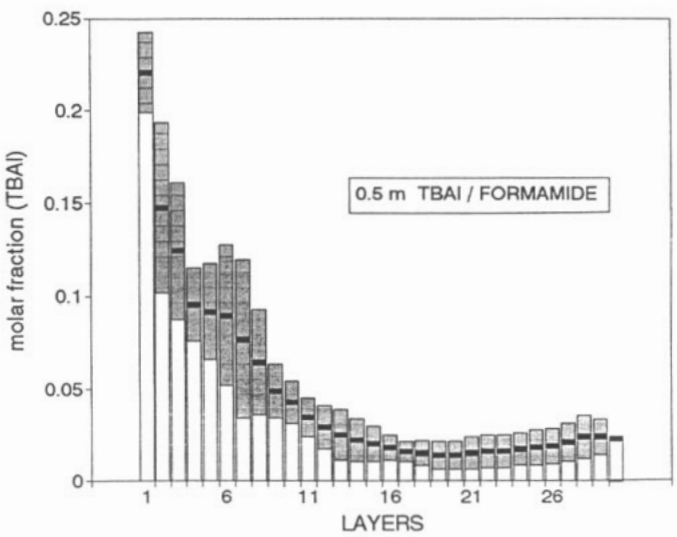

Figure 5. Concentration–depth profile expressed as TBAI molar fraction in 30 layers. The last layer represents the bulk value. The shaded areas represent the standard deviation as explained in section 3.3. The spatial thickness d_j of the layers is neither constant nor a well defined quantity. A rough measure is $d_j \simeq 1.5$ Å.

As the mean free path $\lambda(E_{XPS})$ is about 30 Å, every layer has a thickness of $d = \lambda(E_{XPS})t(E_{XPS}) = 1.5$ Å, even though this is not a well defined quantity in the present theory. However, a crude estimate is sufficient for the following consideration; it appears surprising that the concentration of TBAI drops so sharply from the topmost layer to the deeper layers. On the scale of the layer thickness of about 1.5 Å the TBAI molecule is a rather bulky object of about 10 Å diameter. So how can it have a comparatively low concentration in the fourth layer when it is present so abundantly in the first? It is possible to rationalize this observation if one realizes that the experimental data evaluated here refer to the relative abundance of C 1s atoms in TBAI and in FA. Thus, we cannot speak of having a high concentration of TBAI molecules in the first layer, but only of a high concentration of TBAI-related carbon atoms. We may conclude that the tetrahedral TBA^+ ions have a preferred orientation near the surface; three of the four–$(CH_2)_3CH_3$ alkane groups turn

up at the surface itself whereas only one hydrocarbon chain points into the solvent. The hydrophobic character of the alkane groups would be in agreement with this notion. Such a situation is illustrated in figure 6. We may even discuss the question whether our results would support complete orientation. If so, we would expect three quarters of the TBA^+ carbon atoms immediately at the surface. For this purpose we evaluate quantity $\Gamma_{TBAI}(j)$, as defined in equation (11), which measures the amount of salt per layer. The corresponding profile is shown in figure 7. It has a similar shape as known from figure 5, even though the enhancement in the top layers is less drastic. From the inspection of this profile it becomes apparent that the above-mentioned orientation cannot uniformly be obeyed by all TBA^+ ions while it clearly is a very likely behaviour of these hydrophobic ions at the surface of the solution.

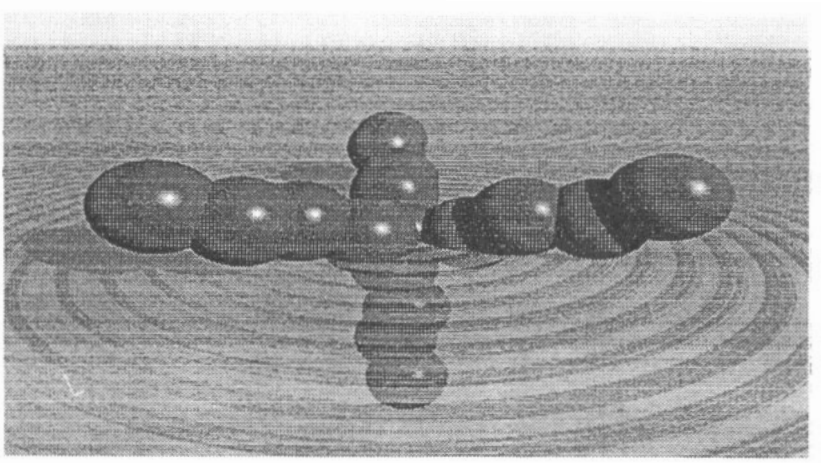

Figure 6. Graphical illustration of the preferred orientation of the TBA^+ ion at the liquid surface. For clarity, except for the TBA^+ ion, all other species in the liquid are shown as a continuum.

Since we have pointed out that in the present formulation of the depth profile the mean free path is not a constant but a function of the local composition, it is interesting to check how serious the effect is. As the mean free path measured in units of length is not a well defined quantity, we express the mean free path as mass per area:

$$\lambda_M(j) = \frac{1}{N_A \sigma_1}\left(\sum_k C_k(j) m_k\right) \Big/ \left(\sum_k C_k(j)\frac{\sigma_k}{\sigma_1}\right) \tag{24}$$

with m_k denoting the molar weight of species k, and N_A Avogadro's number. The index $k = 1$ refers to FA and $k = 2$ to TBAI. In figure 8 we have plotted this quantity for the electron energy $E_{XPS} = 1200$ eV. $\lambda_M(j)$ remains fairly constant in spite of the varying composition of the layers. This may be understood in the following way: even though the salt contains the heavy element iodine it overwhelmingly consists of second-row elements and hydrogen, as does the solvent. At least in the gas phase [14], electron impact cross sections of organic molecules depend within a few per cent on only one parameter, namely the number of electrons. This holds for electron energies between 10 and 3000 eV [14], at least as far as ionization is concerned. At high electron energies, i.e. above several hundred electronvolts, ionization is the dominant inelastic channel. At lower energies, electronic

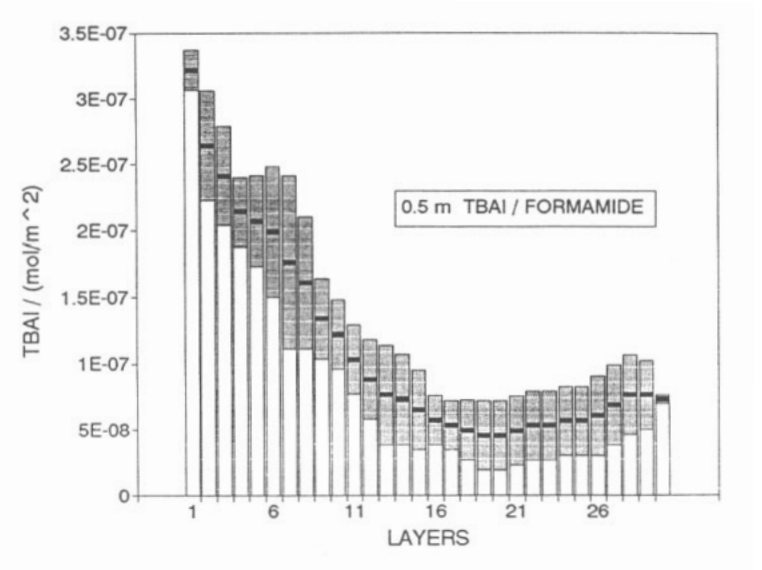

Figure 7. Concentration depth profile expressed as amount TBAI per layer. The amount is given in units of mol m^{-2}. Otherwise as figure 5.

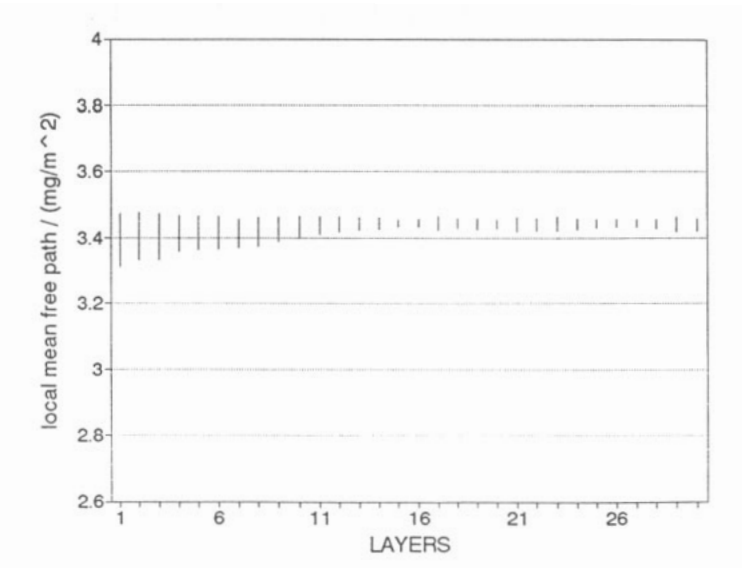

Figure 8. The mean free path for the layers, given in units of mg m^{-2}.

excitation of the target molecules plays a role, too. We may assume, however, that among different organic molecules the total cross section for inelastic energy loss scales with the number of electrons of the molecules as is the case for the ionization channel alone.

From our parameter $\lambda(E)/\lambda(E_{XPS})$ introduced in equation (8) we derive via equation (17) the energy dependence of the inelastic energy loss cross section of a FA molecule in the liquid phase. The result is shown in figure 9. For comparison we have plotted the experimental electron impact ionization cross section of the organic molecule propene which has the same number of 24 electrons as FA and thus should have a very

similar cross section [14]. At high energies we find very good agreement. It is noteworthy that both data sets are absolute values. Below 100 eV electron energy, electronic excitation appears to become increasingly dominant over ionization as the source for electron energy loss.

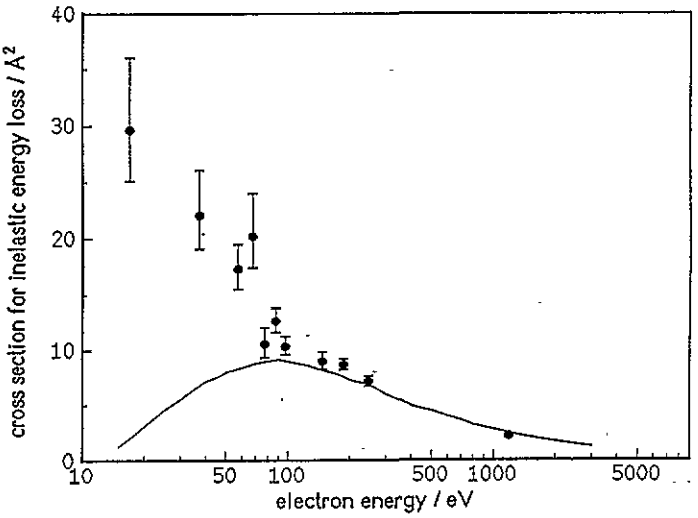

Figure 9. Cross section for inelastic energy loss of electrons by one FA molecule in liquid FA. The error bars result from the standard deviation of the energy-dependent mean free paths. The full curve represents the experimental electron impact ionization cross section of propene [14], an organic molecule with the same number of electrons as FA. For further discussion see text.

5. Summary

From our large set of ARUPS data taken at the surface of a 0.5 M solution of TBAI in FA we derive a concentration–depth profile of the salt.

We find a range of about 12 Å thickness with a markedly enhanced salt concentration. At larger separation z from the surface we observe a zone between $z \simeq 20$ Å and $z \simeq 40$ Å where the salt is slightly but significantly depleted as against the bulk concentration.

The distribution of the TBA^+ carbon atoms within the salt-rich overlayer suggests that the cations have a preference for a particular orientation; three of the four–$(CH_2)_3CH_3$ chains of the ammonium ion are outside the solvent whereas only one alkane group points into the bulk. This orientation, while being most probably energetically preferred, is not exclusive, however.

Together with the concentration profile we determine several other interesting pieces of information: the mean free path of electrons in liquid FA as a function of electron energy between 17 and 1200 eV, the ratio of the inelastic electron energy loss cross sections for TBAI to that of FA and an absolute value for the energy loss cross section of electrons per FA molecule in the liquid state.

Acknowledgments

This work has been made possible by generous financial support from the Ministry for Research and Technology (BMFT) under 05 442AAB 5 and 05 5PWAAI 0. The German Science Foundation (DFG) has sponsored part of the work within the grant Mo 288/15-1. M Wulf helped to collect some of the data at BESSY. J Oberbrodhage prepared figure 6.

References

[1] Ballard R E, Jones J and Sutherland E 1984 *Chem. Phys. Lett.* **112** 310
[2] Holmberg S, Moberg R, Zhong C Y and Siegbahn H 1986 *J. Electron. Spectrosc. Relat. Phenom.* **41** 337
[3] Holmberg S, Zhong C Y, Moberg R and Siegbahn H 1988 *J. Electron. Spectrosc. Relat. Phenom.* **47** 27
[4] Morgner H, Oberbrodhage J, Richter K and Roth K 1991 *J. Phys.: Condens. Matter* **3** 5639
[5] Oberbrodhage J 1992 *PhD Thesis* Witten
[6] Morgner H and Oberbrodhage J 1994 *J. Phys.: Condens. Matter* to be published
[7] Morgner H 1994 *J. Electron. Spectrosc. Relat. Phenom.* **68** 771
[8] Rudolph G and Schwefel H P 1994 *Physica* B1 **50** 236
Brand F 1994 *Physica* B1 **50** 344
[9] Müller W 1986 *PhD Thesis* Freiburg
[10] Morgner H 1993 *Low Energy Electrons for the Investigation of Liquid Surfaces (Proc. NATO Adv. Study Inst.) (Patras, 1993)* ed E Illenberger and W F Schmidt
[11] Baschenko O A 1991 *J. Electron. Spectrosc. Relat. Phenom.* **57** 297
[12] Morgner H and Siegbahn H O G 1994 to be published
[13] Baschenko O A, Bökman F, Bohman O and Siegbahn H O G 1993 *J. Electron. Spectrosc. Relat. Phenom.* **62** 317
[14] Nishimura H and Tawara H 1994 *J. Phys. B: At. Mol. Phys.* **27** 2063
[15] Adamson A W 1982 *Physical Chemistry of Surfaces* (New York: Wiley)
[16] Becks K H, Hahn S and Hemker A 1994 *Physica* B1 **50** 238
[17] Holland J H 1992 *Spektrum Wissenschaft* **9** 44